MCB
Journals.ASM.org

A Single Conserved Residue Mediates Binding of the Ribonucleotide Reductase Catalytic Subunit RRM1 to RRM2 and Is Essential for Mouse Development

Julia Specks,[a] Emilio Lecona,[a] Andrés J. Lopez-Contreras,[b] Oscar Fernandez-Capetillo[a,c]

Genomic Instability Group, Spanish National Cancer Research Center, Madrid, Spain[a]; Center for Chromosome Stability, Department of Cellular and Molecular Medicine, Panum Institute, University of Copenhagen, Copenhagen, Denmark[b]; Science for Life Laboratory, Division of Translational Medicine and Chemical Biology, Department of Medical Biochemistry and Biophysics, Karolinska Institute, Stockholm, Sweden[c]

The ribonucleotide reductase (RNR) complex, composed of a catalytic subunit (RRM1) and a regulatory subunit (RRM2), is thought to be a rate-limiting enzymatic complex for the production of nucleotides. In humans, the *Rrm1* gene lies at 11p15.5, a tumor suppressor region, and RRM1 expression in cancer has been shown to predict responses to chemotherapy. Nevertheless, whether RRM1 is essential in mammalian cells and what the effects of its haploinsufficiency are remain unknown. To model RNR function in mice we used a mutation previously described in *Saccharomyces cerevisiae* (Rnr1-W688G) which, despite being viable, leads to increased interaction of the RNR complex with its allosteric inhibitor Sml1. In contrast to yeast, homozygous mutant mice carrying the *Rrm1* mutation (*Rrm1*$^{WG/WG}$) are not viable, even at the earliest embryonic stages. Proteomic analyses failed to identify proteins that specifically bind to the mutant RRM1 but revealed that, in mammals, the mutation prevents RRM1 binding to RRM2. Despite the impact of the mutation, *Rrm1*$^{WG/+}$ mice and cells presented no obvious phenotype, suggesting that the RRM1 protein exists in excess. Our work reveals that binding of RRM1 to RRM2 is essential for mammalian cells and provides the first loss-of-function model of the RNR complex for genetic studies.

Replication stress (RS) refers to a variety of situations that lead to the accumulation of unprotected single-stranded DNA (ssDNA) at stalled replication forks. Due to the recombinogenic nature of ssDNA, it is a source of genomic rearrangements frequently observed in cancer (1). One way by which ssDNA can accumulate at replication forks is by reduced deoxynucleoside triphosphate (dNTP) concentrations, which limit the progression of the DNA polymerases. Accordingly, reduced dNTP levels have been proposed as a source of genomic instability in cancer (2). In mammals, RS is signaled and suppressed by a phosphorylation cascade that is initiated by the ATR kinase (3, 4). Although how this signaling cascade suppresses RS is not entirely understood, evidence from yeast and more recently from mouse models suggests that it might be linked to a role of ATR in the regulation of nucleotide pools (5–7).

In all eukaryotes, dNTP production involves a rate-limiting ribonucleotide reductase (RNR) complex, which reduces nucleoside diphosphates (NDPs) to deoxyribonucleoside diphosphates (dNDPs) (8). The complex is a heterotetramer formed by two identical subunits, each of which is made of a catalytic subunit (RRM1; Rnr1 in *Saccharomyces cerevisiae*) and a regulatory subunit (RRM2; Rnr2 in yeast). RRM1 contains the catalytic site as well as two allosteric sites for its regulation. The smaller RRM2 subunit carries a nonheme iron center (Fe-O-Fe) that is used for the oxygen-dependent generation of a stable tyrosyl radical necessary for the reduction step. During catalysis, this radical is shuttled to redox-active cysteines in the RRM1 active site (8). The active site, oxidized and inactive after this step, becomes subsequently activated by rereduction of the cysteines via interaction with the RRM1 C-terminal domain (CTD) of the neighboring RRM1 subunit, preparing it for a new cycle of catalysis (9). Given the mutagenic effects of imbalanced dNTP pools (10–12), multiple levels of regulation limit RNR activity until it is needed, namely, during DNA replication and repair.

RNR activity starts to rise at the G_1/S border, resulting in about a 10-fold increase of dNTP levels during S phase, which sharply decrease before cells enter into mitosis (13). In mammals, whereas RRM1 levels remain stable throughout the cell cycle, RRM2 is expressed only during S phase and is degraded by the anaphase-promoting complex (APC) in G_0/G_1 and M phases (reviewed in reference 8). In addition, an alternative and p53-inducible small subunit, RRM2B, can bind RRM1 to provide additional dNTPs for mitochondrial replication and DNA repair (14, 15). While the main fraction of the RNR subunits localizes to the cytosol, small fractions of both proteins can be found in the nucleus in response to DNA damage (16). In addition to the regulated expression of RNR subunits, yeast cells also contain allosteric inhibitors of the RNR. In budding yeast (*S. cerevisiae*) a small protein inhibitor, Sml1, binds and inhibits the RNR by preventing the interaction between both Rnr1 subunits that is essential for reactivation of the RNR (6, 9, 17). Interestingly, activation of the ATR orthologue Mec1 leads to the degradation of Sml1 (18), which increases RNR

Received 11 May 2015 **Returned for modification** 5 June 2015
Accepted 11 June 2015

Accepted manuscript posted online 15 June 2015

Citation Specks J, Lecona E, Lopez-Contreras AJ, Fernandez-Capetillo O. 2015. A single conserved residue mediates binding of the ribonucleotide reductase catalytic subunit RRM1 to RRM2 and is essential for mouse development. Mol Cell Biol 35:2910–2917. doi:10.1128/MCB.00475-15.

Address correspondence to Oscar Fernandez-Capetillo, ofernandez@cnio.es.

doi:10.1128/MCB.00475-15

activity. Moreover, deletion of Sml1 can rescue the viability of *mec1*Δ mutants, strongly suggesting that the essential role of ATR is linked to RNR activity (6). A recent study described a human protein, IRBIT, with distant sequence homology to Sml1 in a small peptide, that could bind and inhibit the RNR. However, this interaction was limited to mitosis and to RRM1/RRM2B complexes, which is different from the general role that Sml1 plays in inhibiting the RNR (19). Although RNR subunits are highly conserved from yeast to humans, including the sequence where Sml1 binds to Rnr1, and although recombinant yeast Sml1 may bind and inhibit the mammalian RNR (17, 18), no allosteric inhibitors of the canonical RRM1/RRM2 complex have been described in mammals.

In 2010, Rothstein and colleagues reported a point mutation in *S. cerevisiae rnr1* (Rnr1-W688G) that leads to a specific increase in Sml1 binding to Rnr1, resulting in reduced RNR activity, dNTP levels, and cell viability, all of which could be rescued by concurrent depletion of Sml1 (20). We hypothesized that if a mammalian orthologue of Sml1 were to exist, introducing this mutation into the mouse genome might lead to increased binding of such a factor to RRM1. The altered mice should have constitutively lower levels of nucleotides, providing a valuable model to explore the impact of reduced nucleotide pools in mammalian health. Hence, given that the sequence surrounding Rnr1 W688 (W684 in mice) is conserved from yeast, we generated mice carrying the corresponding mutation. The mutation yielded a nonfunctional RRM1, which, in contrast to what happens in yeast, was not compatible with cellular viability. Even when we were able to purify mammalian RNR complexes, proteomic analyses failed to detect any protein that bound more avidly to RRM1 carrying the W684G (RRM1-WG) mutation. In contrast to the mechanism reported in yeast, the mutation in mice prevents the binding of RRM1 to RRM2, demonstrating that RNR complex formation is essential for mammalian cellular viability. Finally, the lack of detectable phenotypes in RRM1 heterozygous mutant mice suggests that RRM1 exists in excess in mammalian cells and argues against a major tumor-suppressive role of RRM1 heterozygosity.

MATERIALS AND METHODS

Mouse work. For the generation of the *Rrm1*^{WG} allele, a 16.8-kb region from the mouse genome containing *Rrm1* was first cloned from a bacterial artificial chromosome (BAC RP23-111K8) into a minimal vector and subsequently mutagenized by recombineering (Gene Bridges). The linearized vector was electroporated into murine embryonic stem (mES) cells by the Transgenic Mice Unit of the Spanish National Cancer Center (Centro Nacional de Investigaciones Oncológicas [CNIO]). Properly recombined mES cells were identified by Southern blotting through standard procedures and subsequently used for the generation of chimeric mice. Knock-in mice were genotyped by PCR with primers amplifying a 369-bp sequence from the vector (available upon request). Mice were kept under standard conditions at a specific-pathogen-free facility of the Spanish National Cancer Center in a mixed C57BL/6-129/Sv background. All mouse work was performed in accordance with the Guidelines for Humane Endpoints for Animals Used in Biomedical Research and under the supervision of the Ethics Committee for Animal Research of the Instituto de Salud Carlos III.

Irradiation. Sublethal irradiation (6 Gy of total-body ionizing radiation [IR]) was administered to 8-week-old mice (RS 2000 X-ray biological irradiator; 160 kV, 4.2 kW, 25 mA [Rad Source]). Hematologic parameters were evaluated at 1 to 5 weeks postirradiation as indicated below.

Blood analysis. Blood samples were obtained from the sublingual vein. Samples were collected in EDTA-treated microtubes (Aquisel) and run on an Abacus Junior Vet hematology analyzer (Diatron), which provides complete blood analyses, including counts of leukocytes and platelets.

Cell culture. 293 and U2OS cells were grown in Dulbecco's minimum essential medium (DMEM; Invitrogen) supplemented with 10% fetal bovine serum (FBS; Lonza) and 1% penicillin-streptomycin. Mouse embryonic fibroblasts (MEFs) from embryonic day 13.5 (E13.5) embryos were generated by standard methods and grown in DMEM supplemented with 15% FBS. For all experiments, MEFs were used at low passage numbers (<3) and grown in 5% oxygen to minimize exposure to reactive oxygen species. Splenic B cells were isolated with anti-CD43 microbeads (anti-Ly48; Miltenyi Biotech) and cultured in the presence of 25 μg/ml lipopolysaccharide (LPS; Sigma). Hydroxyurea (HU; Sigma) was added at the concentrations indicated in the figure legends.

Plasmid construction. For the construction of pcDNA5/FRT/TO-RRM1 (where FRT is Flp recombination target) with a C-terminal streptavidin (Strep) tag, the coding sequence of human RRM1 (hRRM1) was amplified by PCR from human cDNA and cloned into pEXPR-IBA103 (Novagen) vector at SacII/XhoI sites. From there, the Strep-RRM1 sequence was PCR amplified, adding AflII/NotI restriction sites for subsequent cloning into the pcDNA 5/FRT/TO vector (Life Technologies). Expression plasmids for RRM1 with the W684G mutation (RRM1-WG) were constructed by introducing the W684G mutation into the wild-type (wt) pEXPR-IBA103 expression plasmid using a QuickChange site-directed mutagenesis kit (Agilent Technologies), followed by PCR and subcloning into the pcDNA 5/FRT/TO vector as described above. The final constructs were sequenced to rule out the presence of mutations. For bacterial expression, the cDNAs of human RRM1, RRM1-WG, RRM2, and RRM2B were cloned into the pET30a expression vector at SalI/NotI (RRM1 and RRM1-WG) or BamHI/XhoI (RRM2 and RRM2B) RS sites and expressed as 6×His-tagged versions. In addition, RRM1 and RRM1-WG were expressed as Strep-tagged versions by removal of the N-terminal His tag and introduction of a Strep tag into the pET30a vector.

Protein expression. Stable cell lines of Flp-In T-REx 293 cells (Life Technologies) expressing mutant or wt RRM1 were generated according to the manufacturer's instructions. Recombinant protein expression was induced by addition of 100 ng/ml doxycycline to the medium for the times indicated in the figure legends. In addition, RRM2, RRM2B, RRM1, and RRM1-WG were expressed in *Escherichia coli* BL21(DE3) (Life Technologies). Cells were grown in Terrific broth (TB) medium at 37°C until the culture reached an optical density at 600 nm (OD_{600}) of 0.6. Cells were then chilled to 15°C for 30 min and induced with 0.5 mM isopropyl-β-D-thiogalactopyranoside (IPTG) for 18 h at 15°C with shaking at 220 rpm. Cells were harvested by centrifugation at 5,000 × *g* for 30 min, and pellets were stored at −80°C.

Immunoblotting. For whole-cell extracts, cells were washed once with phosphate-buffered saline (PBS) and lysed in radioimmunoprecipitation assay (RIPA) buffer (50 mM Tris-HCl, pH 7.4, 1% NP-40, 0.25% Na-deoxycholate, 150 mM NaCl, 1 mM EDTA) containing protease and phosphatase inhibitors (Sigma). Cytosolic and nuclear extracts were prepared as previously described (21). Samples were resolved by SDS-PAGE and analyzed by standard Western blotting (WB) techniques. Antibodies against Strep-tag II (71590-3; Novagen), RRM2B (ab8105; Abcam) RRM2 (Sc-10844; Santa Cruz), RRM1 (3388; Cell Signaling), β-actin (A5441; Sigma), Chk1 (Novocastra), Chk1 phosphorylated at S345 (Chk1-S345P) (2348S; Cell Signaling Technology), replication protein A (RPA) (ab2175; Abcam), RPA-S4P/S8P (S4/S8) (A300-245A; Bethyl), and γH2AX (05-636; Upstate) were used.

IP. For protein immunoprecipitation (IP) from Flp-In T-REx 293 cells, cell lysate was loaded on a Bio-Spin disposable chromatography column (Bio-Rad) and incubated with Strep-Tactin Macroprep resins (Iba) for 2 h at 4°C on a rotator. The column was washed five times with buffer W (100 mM Tris-HCl, pH 8, 1 mM EDTA, 200 mM NaCl) containing 0.1% NP-40. RRM1 or RRM1-WG and associated proteins were eluted with buffer W containing 2 mM biotin. For the isolation of recom-

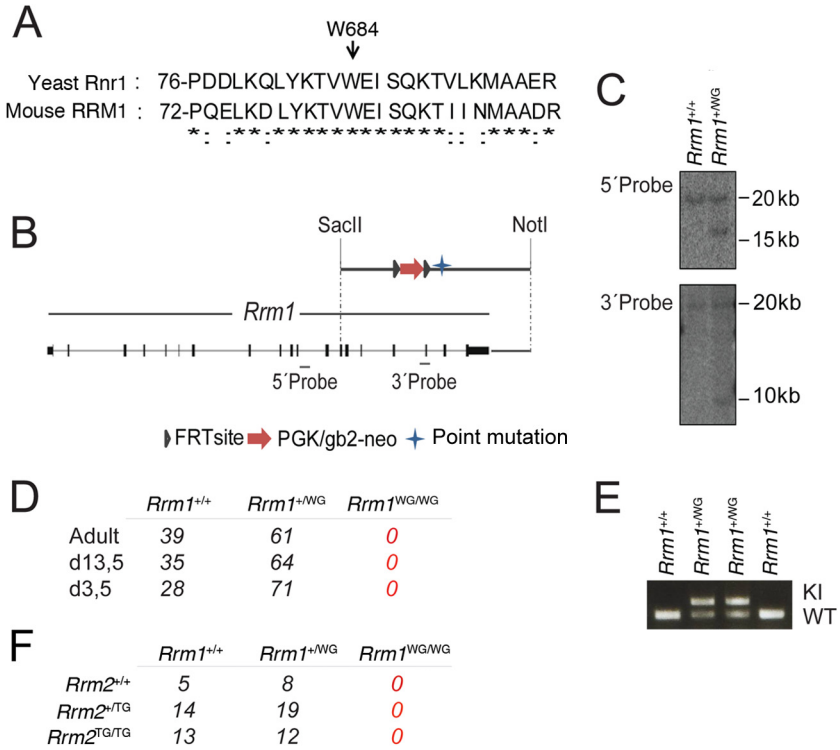

FIG 1 Embryonic lethality in *Rrm1*$^{WG/WG}$ mice. (A) Pairwise local alignments of yeast (*Saccharomyces cerevisiae*) and mouse (*Mus musculus*) RRM1 protein sequences surrounding W684. (B) Scheme of the *Rrm1* knock-in construct harboring a neomycin resistance cassette (PGK/gb2-neo) flanked by FRT sites and a point mutation in exon 18 (W688G). The mutation is flanked by two homology arms of 6 kb. (C) Southern blotting in murine embryonic stem cells (mES) electroporated with the construct shown in panel A. Probes external (5′ Probe) and internal (3′ Probe) to the construct were used to confirm the presence of a single correct integration site in the mES cells. The 20-kb band corresponds to the untargeted *Rrm1* allele in *Rrm1*$^{+/WG}$ cells. (D) Table showing the expected and observed genotypes of 3-week-old pups, MEFs, or mES cells obtained from crosses of *Rrm1*$^{+/WG}$ animals. d13.5, 13.5 days postcoitus; d3.5, 3.5 days postcoitus. (E) Example of the genotyping of PCR products illustrating the only two genotypes that were obtained from crosses of *Rrm1*$^{+/WG}$ animals. WT, wild type; KI, knock-in. (F) Table showing the observed genotypes of 3-week-old pups obtained from crosses of *Rrm1*$^{+/WG}$ *Rrm2*$^{+/TG}$ animals. TG, transgenic.

binant protein from bacteria, cells were thawed on ice and resuspended in 50 mM Tris (pH 7.8), 200 mM NaCl, 2 mM phenylmethylsulfonyl fluoride (PMSF), and 1 mM dithiothreitol (DTT). Cells were ruptured by sonication cycles at 4°C and centrifuged at 30,000 × *g* for 30 min at 4°C. The supernatant was incubated with Ni-nitrilotriacetic acid (NTA)–agarose (Qiagen) or Strep-Tactin Macroprep resins for 1 h at 4°C on a rotator and loaded onto a Bio-Spin disposable chromatography column. For purification of Strep-tagged proteins, beads were washed three times with 50 mM Tris (pH 7.8), 200 mM NaCl, 2.5 mM, and 2 mM PMSF, and bound protein was eluted with buffer containing 2 mM biotin. For the purification of His-tagged proteins, 10 mM imidazole was added to the washing buffer, and samples were eluted in buffer containing 250 mM imidazole. Fractions were analyzed for purity using a 12% SDS-PAGE gel and Coomassie staining. Fractions containing RRM1, RRM1-WG, RRM2, or RRM2B were pooled and dialyzed against 50 mM Tris (pH 7.8), 200 mM NaCl, 2.5 mM, 2 mM PMSF, and 10% glycerol, and purified proteins were stored at −80°C.

***In vitro* binding assay.** A total of 1.5 μg of Strep-RRM1 or Strep-RRM1-WG and 1.5 μg of His-RNR subunits were mixed in 0.5 ml of IP buffer (25 mM Tris-HCl, pH 7.5, 200 mM NaCl, 1 mM EDTA, 2 mM PMSF, 1 mM DTT) and incubated for 20 min at room temperature (RT). Strep-Tactin beads were added, and samples were incubated for 1.5 h under constant rotation at 4°C. Beads were washed five times, and bound proteins were eluted in IP buffer containing 2 mM biotin. Proteins were separated on an SDS gel and stained with Coomassie or analyzed by WB.

HTM analyses. For high-throughput microscopy (HTM) analyses, cells were grown on μCLEAR flat-bottom 96-well plates (Greiner Bio-One), and γH2AX immunofluorescence was performed using standard procedures. Images were automatically acquired from each well by an Opera high-content screening system (PerkinElmer). A 20× magnification lens was used, and pictures were taken under nonsaturating conditions. Images were segmented using 4′,6′-diamidino-2-phenylindole (DAPI) staining to generate masks matching cell nuclei from which the average γH2AX signal was calculated. Data are represented with the use of Prism software (GraphPad Software).

RNA isolation and real-time PCR. Total RNA was isolated using an Absolutely RNA Microprep kit (Stratagene) according to manufacturer's recommendations. cDNA was synthesized using a SuperScript II Reverse Transcriptase kit for reverse transcription-PCR (RT-PCR; Invitrogen). Real-time PCR was performed using SYBR-Greener quantitative PCR (qPCR) supermix (Invitrogen) in a real-time PCR system (Bio-Rad). The glyceraldehyde-3-phosphate dehydrogenase (GAPDH) expression level was used to normalize values of gene expression. Data are shown as fold change relative to the level of the sample control, and at least two independent experiments in triplicate were performed. Primers are available upon request.

Flow cytometry. Cells were resuspended in a PBS solution containing 1% (wt/vol) bovine serum albumin (BSA), 10 μg/ml propidium iodide, and 0.5 mg/ml RNase A and were analyzed by flow cytometry in a FACSCalibur machine (BD).

RESULTS AND DISCUSSION

The Rrm1-W684G mutation causes early embryonic lethality in mice. In order to evaluate the consequences of the W688G change encoded by *rnr1* (*rnr1-W688G*) in mammals, we gener-

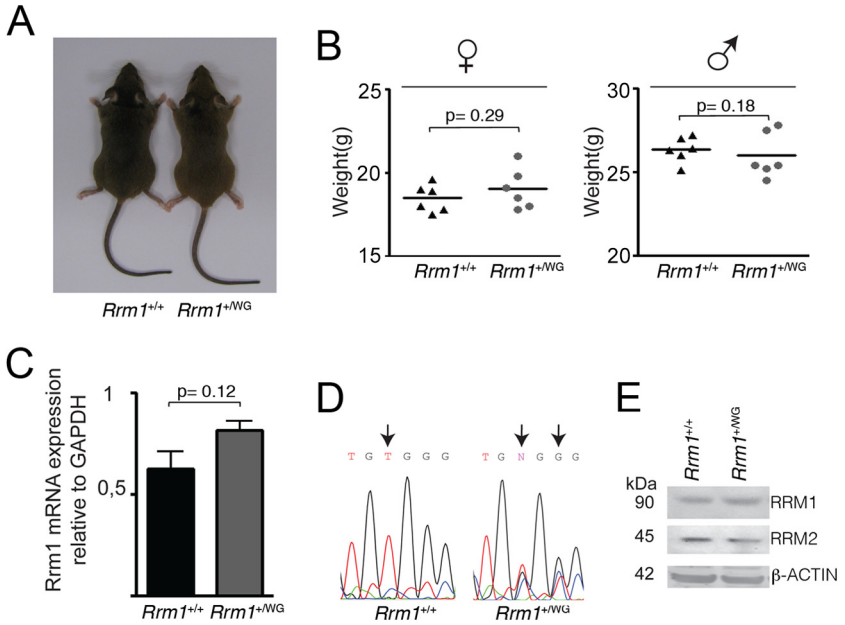

FIG 2 Normal RRM1 expression in *Rrm1*$^{+/WG}$ mice. (A) Representative picture of 4-month-old wt and *Rrm1*$^{+/WG}$ littermates. (B) Weight distribution of 2-month-old wt and *Rrm1*$^{+/WG}$ mice. (C) Real-time PCR (RT-PCR) analysis of *Rrm1* mRNA levels in wt and *Rrm1*$^{+/WG}$ MEFs. Results are representative of three independent experiments performed in triplicate. (D) Chromatogram of sequenced *Rrm1* RT-PCR products obtained in the experiment described for panel C. The arrows indicate the positions of the mutations (TGG → GGC) introduced in the *Rrm1*^{WG} allele. (E) Western blot showing the levels of RRM1 and RRM2 in purified wt and *Rrm1*$^{+/WG}$ B cells after a 2-day stimulation with lipopolysaccharide from wt and *Rrm1*$^{+/WG}$ mice. β-Actin is shown as a loading control. No significant differences were found between the results of any of the analyses shown in the figure.

ated knock-in mice carrying the corresponding W684G mutation encoded by the *Rrm1* gene. To this end, a 16.8-kb region of *Rrm1* containing exons 14 to 19 was subcloned from a BAC and subsequently mutated at the W684 position by recombineering (Fig. 1A and B). The construct was subsequently used for the electroporation of mouse embryonic stem (mES) cells, which were selected for correct integration of the mutant sequence by Southern blotting (Fig. 1C). Properly recombined ES lines were used for the generation of mouse founder lines carrying the mutation using standard procedures. Given that the targeting construct carried a neomycin resistance cassette flanked by FRT sites, *Rrm1* mutant mice were initially crossed with a transgenic mouse strain that ubiquitously expresses flippase (22), which enabled the deletion of the neomycin cassette, leaving exclusively the W684 mutation and an intronic FRT site in the final allele (*Rrm1*^{WG}).

Although no obvious phenotypes were observed in *Rrm1*$^{+/WG}$ mice, no *Rrm1*$^{WG/WG}$ mice were born, nor were we able to detect homozygous mutant embryos at 13.5 or 10.5 days postcoitus (dpc) (Fig. 1D and E). We also failed to generate homozygous mutant ES lines from 3.5-dpc blastocysts, further underscoring the essential nature of the mutation. Given the limiting role of RRM2 levels for RNR activity in mammals, we sought to rescue *Rrm1*$^{WG/WG}$ lethality by crossing *Rrm1* mutant heterozygous animals with a transgenic mouse strain we recently generated that harbors increased RRM2 levels and supraphysiological RNR activity (7). However, increased RRM2 expression failed to rescue the viability of RRM1 mutant animals (Fig. 1F). Collectively, these results reveal that the W684 residue of RRM1 is essential for mammalian cellular viability in a manner that cannot be rescued by an additional supply of RRM2.

Rrm1$^{+/WG}$ mice present normal RRM1 levels and a proficient RS response. In contrast to *Rrm1*$^{WG/WG}$ mice, *Rrm1*$^{+/WG}$ mice were fertile, born at the expected ratios, and showed no obvious phenotype (Fig. 2A and B). To determine if the essential nature of the *Rrm1-W684G* mutation was due to an effect on protein levels, we first verified whether *Rrm1*$^{+/WG}$ cells presented normal expression of the mutant allele. RT-PCR followed by sequencing revealed equivalent expression levels of the mutant and wild-type (wt) mRNAs in *Rrm1*$^{+/WG}$ cells (Fig. 2C and D). Moreover, Western blotting (WB) also failed to show any noticeable differences in RRM1 protein levels between wt and heterozygous cells (Fig. 2E). Hence, wt and RRM1-W684G (here, RRM1-WG) versions of RRM1 coexist at similar levels in *Rrm1*$^{+/WG}$ cells.

To overcome the limitations imposed by the lethality of the mutation in mice and to further explore the consequences of RRM1-WG expression in mammals, we developed a human cell line where the expression of wt or mutant RRM1 proteins could be induced by doxycycline (Fig. 3A). In agreement with the absence of obvious phenotypes in *Rrm1*$^{+/WG}$ mice, overexpression of RRM1-WG did not affect the phosphorylation of histone H2AX that is induced upon exposure to the RNR inhibitor hydroxyurea (HU) (Fig. 3B), nor did it have an obvious effect on cell viability or cell cycle progression (Fig. 3C). The subcellular distribution and stability of RRM1-WG were also comparable to those of the wt RRM1 (Fig. 3D and E). Altogether, these results indicate that lethality of *Rrm1*$^{WG/WG}$ mice is not due to lower levels, altered distribution, or intrinsic toxicity of the RRM1-WG protein.

Despite the overall normal appearance of *Rrm1*^{WG} heterozygous mice and given the lethality of the mutation in homozygosis, we next explored whether RNR function was even slightly compromised in *Rrm1*$^{+/WG}$ cells. To investigate this possibility, we

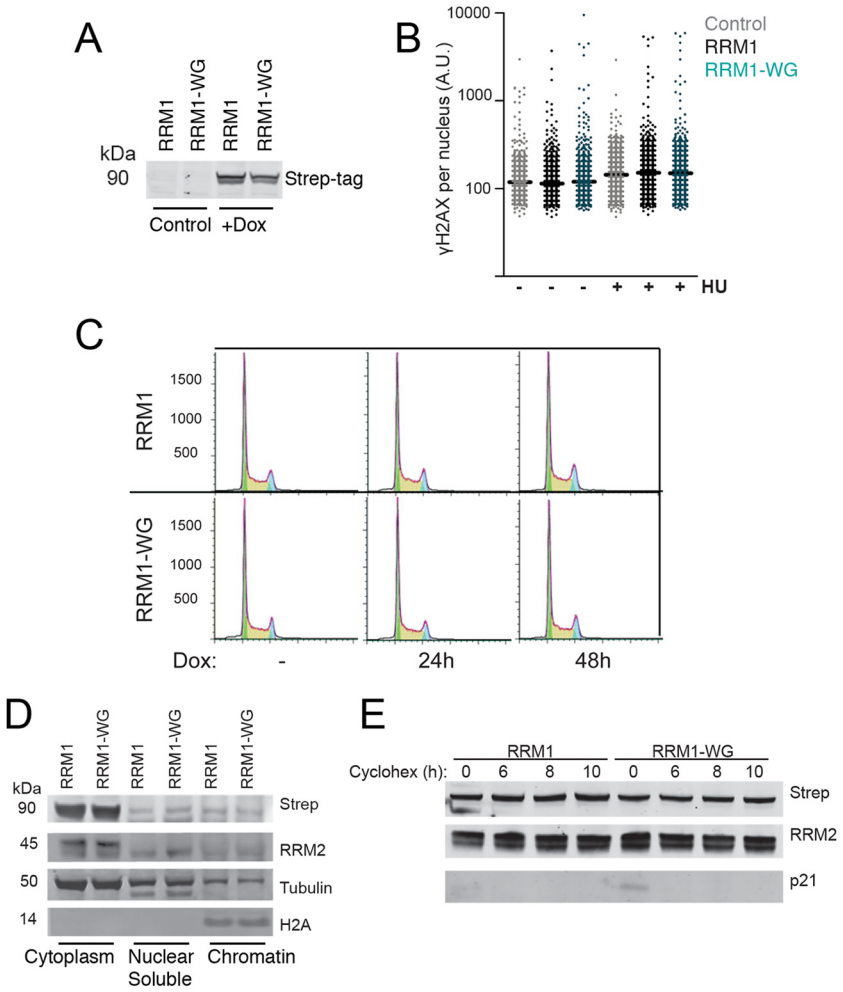

FIG 3 The W684G mutation does not alter the localization or stability of RRM1, nor does it lead to toxic effects when it is overexpressed. (A) WB of Flp-In T-REx 293 cells expressing Strep-RRM1 or Strep-RRM1-WG after 24 h of doxycycline (Dox) induction. (B) Cell cycle profiles of Flp-In T-REx 293 cells expressing RRM1-Strep or RRM1-WG-Strep 24 or 48 h after doxycycline induction. (C) HTM-mediated quantification of γH2AX intensity per nucleus in response to HU (1 mM, 30 min) in U2OS cells 2 days after transfection with plasmids encoding RRM1, RRM1-WG, or an empty vector. No significant differences were found between the results for the different conditions. Data are representative of three independent analyses. AU, arbitrary units. (D) WB analysis of cytoplasmic, nuclear soluble, and chromatin fractions of Flp-In T-REx 293 cells overexpressing Strep-RRM1 or Strep-RRM1-WG 24 h after induction with doxycycline. (E) WB analysis of Flp-In T-REx 293 cells overexpressing Strep-RRM1 or Strep-RRM1-WG at various times after incubation with 25 μg/ml cycloheximide. p21 was used as a control for cycloheximide treatment due to its short protein half-life.

exposed *Rrm1*$^{+/+}$ and *Rrm1*$^{+/WG}$ mouse embryonic fibroblasts (MEFs) to HU. High-throughput microscopy (HTM) revealed that HU-induced γH2AX levels were not altered in *Rrm1*$^{+/WG}$ MEFs compared to those observed in littermate MEFs (Fig. 4A). Of note, this assay is sensitive enough to detect even mild differences in RNR activity (3). Consistent with HTM data, phosphorylation of CHK1 and RPA in response to HU as well as in response to ionizing radiation (IR) was unaffected in *ex vivo* cultures of *Rrm1*$^{+/WG}$ B lymphocytes (Fig. 4B). Finally, given that the hematopoietic stem cell (HSC) compartment is particularly sensitive to nucleotide levels and to RS (23–25), we evaluated the behavior of *Rrm1*$^{+/WG}$ HSCs *in vivo*. To this end, we evaluated how wt and *Rrm1*$^{+/WG}$ HSCs repopulated the bone marrow of mice exposed to a sublethal dose of IR. In agreement with *in vitro* data, hematopoietic recovery of *Rrm1*$^{+/WG}$ and *Rrm1*$^{+/+}$ cells showed no significant differences (Fig. 4C). Collectively, the results above show that the expression of RRM1-WG at around half of the total amount of RRM1 does not have a detectable impact on mammalian cells, supporting the notion that RRM1 exists largely in excess and that RNR activity is mostly dependent on RRM2 levels.

RRM1-WG binds to RRM2 *in vitro* but not *in vivo*. Even if *Rrm1*$^{+/WG}$ mice and cells had no obvious phenotype, the lethality of the allele in homozygosis indicated that the mutant protein was not functional. In yeast, the Rnr1-W688G mutation leads to constitutive binding of the RNR inhibitor Sml1 to Rnr1. The binding of murine RRM1-WG to a yet unidentified RNR inhibitor could also potentially explain the lethality of *Rrm1*$^{WG/WG}$ mice. To search for proteins that more avidly bound to RRM1-WG than to wt RRM1, we purified streptavidin-tagged RRM1 proteins and looked for interactors by mass spectrometry (MS). The purification pipeline was validated since RRM1 and both RRM2 and RRM2B were the proteins identified with the highest number of peptides in these assays. However, no proteins that distinctively bound RRM1-WG (versus RRM1) were

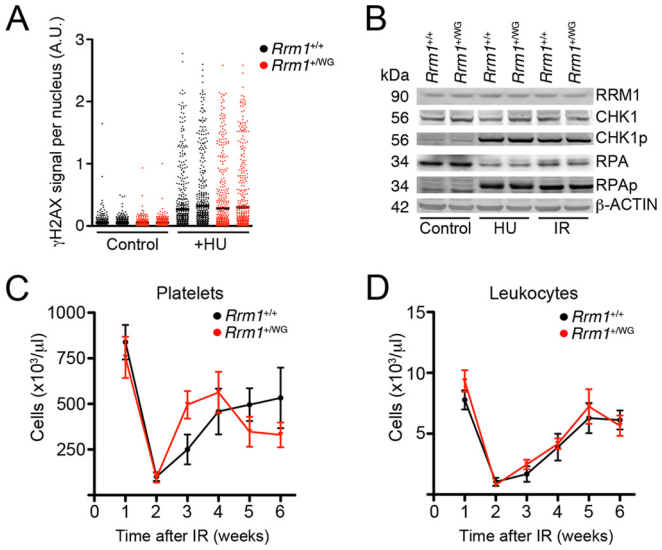

FIG 4 *Rrm1*^{WG} heterozygosity does not impact the responses to DNA damage in cells and mice. (A) HTM-mediated quantification of γH2AX intensities per nucleus in wt and *Rrm1*$^{+/WG}$ MEFs treated with 0.5 mM HU for 4 h. Data from two independent experiments are shown, and the panel is representative of three independent analyses. AU, arbitrary units. (B) RRM1, Chk1p, Chk1, RPA, and RPAp levels measured by WB in wt and *Rrm1*$^{+/WG}$ littermate B cell cultures either untreated (Control) or upon treatment with HU (2 mM, 3 h) or IR (10 Gy, 45 min). Data are representative of two independent analyses. β-Actin was used as a loading control. (C and D) Hematopoietic recovery after a sublethal dose of irradiation (6 Gy). Platelet and leukocyte levels are from wt and *Rrm1*$^{+/WG}$ mice at 1 to 6 weeks postirradiation. Values indicated are means ± standard deviations ($n = 6$). No significant differences were found between results of any of the analyses shown in the figure.

found by MS. In contrast, we observed a major reduction in the number of RRM2 and RRM2B (RRM2/B) peptides that were brought down in RRM1-WG purifications (Fig. 5A). WB confirmed a very significant reduction of the levels of RRM2 and RRM2B in RRM1-WG pulldown assays (Fig. 5B). The incapacity of RRM1-WG to participate in RNR complexes explains both the lethality of *Rrm1*$^{WG/WG}$ mice and the absence of toxic effects of the mutant protein even when it is overexpressed. In addition, it explains the absence of major phenotypes if *Rrm1*$^{+/WG}$ mice and cells since the mutation does not generate a dominant negative version but, rather, an inert RRM1 variant.

While loss of RNR complex formation could explain the lethality observed in *Rrm1*$^{WG/WG}$ mice, this finding stands in contrast to the impact of the mutation in *Saccharomyces cerevisiae*. In yeast, although the Rnr1-W688G mutation led to increased Rnr1-Sml1 binding, the formation of the RNR complex was not compromised. Moreover, deletion of Sml1 rescued the Rnr1-WG phenotypes (20). Interestingly, Chabes and colleagues reported that recombinant yeast Sml1 competes with RRM2 binding to human RRM1, disrupting RNR complex formation (17). Hence, our observation of lower levels of RRM2 in streptavidin-RRM1 pulldown assays allowed two interpretations. The W684G mutation could directly impair the binding of murine RRM1 to RRM2. Alternatively, the mutation could increase the binding of RRM1 to another protein, precluding the RRM1-RRM2 interaction.

To distinguish between these two possibilities, we analyzed the *in vitro* capacity of RRM1-WG to form an RNR complex. To this end, we first expressed and purified mutant and wt RRM1, as well as RRM2 and RRM2B proteins, with an N-terminal His tag from *E. coli*. RRM1 proteins were additionally expressed with an N-terminal Strep tag to allow independent purification. Using purified proteins, we first confirmed that RRM1-WG can bind to wt RRM1 and form the R1 homodimer (Fig. 5C). Second, we tested whether RRM1-WG was able to bind RRM2 or RRM2B *in vitro*. Indeed, recombinant RRM1-WG bound both RNR regulatory subunits as efficiently as wt RRM1 (Fig. 5D). Hence, the introduction of the W684G mutation in murine RRM1 does not intrinsically affect its binding to RRM2 or RRM2B. Finally, to further search for factors that could bind preferentially to RRM1-WG and prevent its binding to RRM2 and given that recombinant proteins were proficient in the formation of an RNR complex, Strep-RRM1 and Strep-RRM1-WG proteins were reversibly linked to Strep-Tactin beads and used as baits for pulldown assays. Once again, MS analyses failed to detect any preferential interactors of RRM1-WG. In contrast and in agreement with our previous approach, recombinant RRM1-WG failed to pull down RRM2 and RRM2B as efficiently as wt RRM1 (Fig. 5E and F). In summary, whereas RRM1-WG can bind to RRM2/B *in vitro*, it fails to form an RNR complex *in vivo*, which explains the lethality of *Rrm1*$^{WG/WG}$ mice.

We here present the characterization of the first loss-of-function mouse model of RRM1, the mammalian catalytic subunit of the RNR. Our approach was based on a recently described mutation in yeast, which led to increased binding of Rnr1 to the RNR inhibitor Sml1. The present work reveals that the mutation also compromises RRM1 function in mice, yet the mechanism differs from that reported in yeast. In mice, the RRM1-W684G mutation prevents the RRM1-RRM2/B interaction, leading to early embryonic lethality. It is possible that the change of a tryptophan residue affects RRM1 binding to other essential proteins, such as the recently described interaction with CHK1 (26), although we failed to detect CHK1 in our analyses. Intriguingly, recombinant RRM1-WG interacts normally with RRM2/B *in vitro*, which raises the question of why the RNR complex does not form *in vivo*. One option is that additional posttranslational modifications (PTM) that occur *in vivo* are responsible for this observation. Alternatively, RRM1-WG could bind to another protein *in vivo*, preventing RRM1 binding to RRM2/B. Unfortunately, we have been unable to find such a factor. Of note, all of our RRM1 or RRM2 pulldown assays failed to identify the recently described RNR inhibitor IRBIT (19), which might be related to the fact that the IRBIT-RNR interaction seems limited to mitosis. Regardless of the *in vitro* binding, the fact that the mutant protein fails to participate in RNR complexes *in vivo* explains the absence of toxic effects of RRM1-WG even when it is overexpressed. Finally, the absence of a phenotype of *Rrm1*$^{+/WG}$ mice, even when they are challenged with DNA damage, indicates that the levels of murine RRM1 are not limiting for RNR function, which would mostly depend on the availability of RRM2. This observation is particularly relevant, given that RRM1 levels are considered a biomarker of sensitivity to chemotherapy in cancer treatment, yet different studies have yielded conflicting results (27). Whereas we do not dispute that severely reduced RRM1 levels might sensitize cells to genotoxic agents, our results indicate that reductions of as much as 50% of RRM1 would have a negligible impact on RNR function, and thus any meaningful changes in expression should further reduce RRM1 expression.

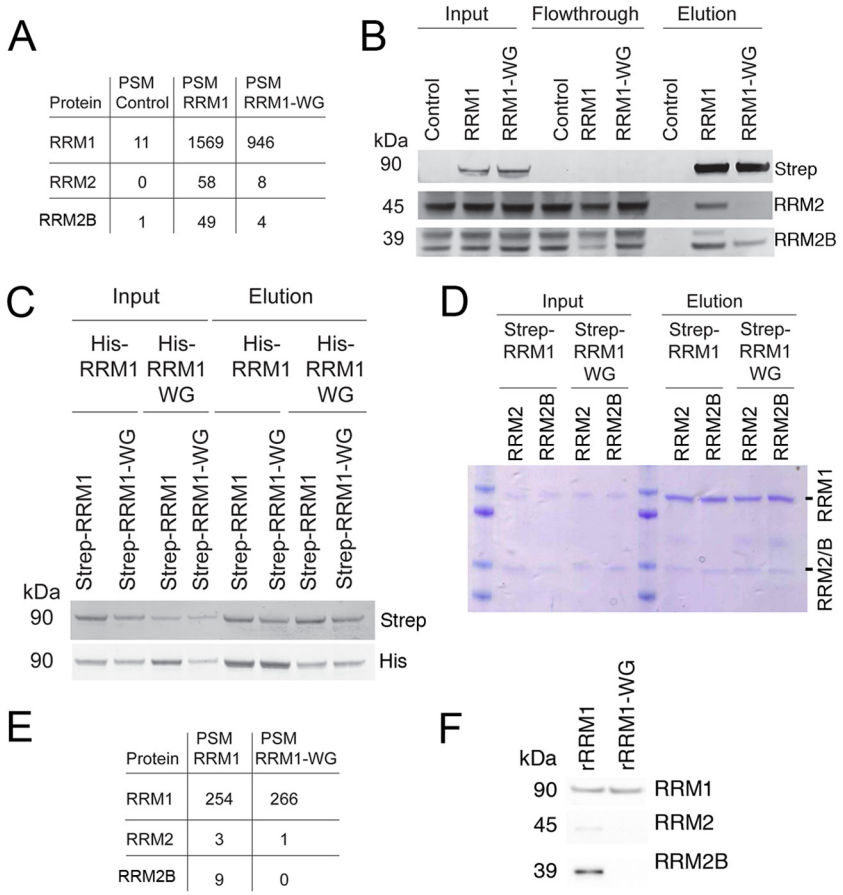

FIG 5 RRM1-WG binds to RRM2/RRM2B *in vitro* but not *in vivo*. (A) Protein spectrum matches (PSM) of RRM1, RRM2, and RRM2B identified by MS in purifications of Strep-RRM1 or Strep-RRM1-WG. (B) Strep IP from total cell lysate of Flp-In T-REx 293 cells overexpressing an empty control vector, RRM1-Strep, or RRM1-WG-Strep proteins. The WB illustrates the efficiency of the purification process. Note that Strep-RRM1 can efficiently pull down RRM2 and RRM2B. (C) *In vitro* incubation of recombinant His-RRM1 or His-RRM1-WG with Strep-RRM1 or Strep-RRM1-WG was followed by Strep IP to verify the formation of RRM1 dimers between the different proteins. (D) *In vitro* incubation of Strep-RRM1 or Strep-RRM1-WG with His-RRM2 or RRM2B was followed by Strep IP to verify the formation of RRM1-RRM2 or RRM1-RRM2B complexes between the different proteins. (E) Protein spectrum matches of RRM1, RRM2, and RRM2B proteins identified by MS in pulldown assays using recombinant Strep-RRM1 or Strep-RRM1-WG. (F) WB illustrating the levels of RRM1, RRM2, and RRM2B from the samples described in panel E.

ACKNOWLEDGMENTS

This research was funded by Fundación Botín, by Banco Santander through its Santander Universities Global Division, and by grants from the Spanish Ministry of Economy and Competitiveness (MINECO; grants SAF2011-23753 and SAF2014-57791-REDC), Worldwide Cancer Research (12-0229), Fundació La Marato de TV3, Howard Hughes Medical Institute, and the European Research Council (ERC-617840) to O.F.-C., by grants from the Danish Council for Independent Research and the Danish National Research Foundation to A.J.L.-C., and by a Ph.D. fellowship from MINECO to J.S. (BES-2012-05 2030).

REFERENCES

1. **Lecona E, Fernandez-Capetillo O.** 2014. Replication stress and cancer: it takes two to tango. Exp Cell Res **329:**26–34. http://dx.doi.org/10.1016/j.yexcr.2014.09.019.
2. **Bester AC, Roniger M, Oren YS, Im MM, Sarni D, Chaoat M, Bensimon A, Zamir G, Shewach DS, Kerem B.** 2011. Nucleotide deficiency promotes genomic instability in early stages of cancer development. Cell **145:**435–446. http://dx.doi.org/10.1016/j.cell.2011.03.044.
3. **Lopez-Contreras AJ, Fernandez-Capetillo O.** 2010. The ATR barrier to replication-born DNA damage. DNA Repair (Amst) **9:**1249–1255. http://dx.doi.org/10.1016/j.dnarep.2010.09.012.
4. **Cimprich KA, Cortez D.** 2008. ATR: an essential regulator of genome integrity. Nat Rev Mol Cell Biol **9:**616–627. http://dx.doi.org/10.1038/nrm2450.
5. **Huang M, Zhou Z, Elledge SJ.** 1998. The DNA replication and damage checkpoint pathways induce transcription by inhibition of the Crt1 repressor. Cell **94:**595–605. http://dx.doi.org/10.1016/S0092-8674(00)81601-3.
6. **Zhao X, Muller EG, Rothstein R.** 1998. A suppressor of two essential checkpoint genes identifies a novel protein that negatively affects dNTP pools. Mol Cell **2:**329–340. http://dx.doi.org/10.1016/S1097-2765(00)80277-4.
7. **Lopez-Contreras AJ, Specks J, Barlow JH, Ambrogio C, Desler C, Vikingsson S, Rodrigo-Perez S, Green H, Rasmussen LJ, Murga M, Nussenzweig A, Fernandez-Capetillo O.** 2015. Increased Rrm2 gene dosage reduces fragile site breakage and prolongs survival of ATR mutant mice. Genes Dev **29:**690–695. http://dx.doi.org/10.1101/gad.256958.114.
8. **Nordlund P, Reichard P.** 2006. Ribonucleotide reductases. Annu Rev Biochem **75:**681–706. http://dx.doi.org/10.1146/annurev.biochem.75.103004.142443.
9. **Zhang Z, Yang K, Chen CC, Feser J, Huang M.** 2007. Role of the C terminus of the ribonucleotide reductase large subunit in enzyme regeneration and its inhibition by Sml1. Proc Natl Acad Sci U S A **104:**2217–2222. http://dx.doi.org/10.1073/pnas.0611095104.
10. **Chabes A, Georgieva B, Domkin V, Zhao X, Rothstein R, Thelander L.** 2003. Survival of DNA damage in yeast directly depends on increased dNTP levels allowed by relaxed feedback inhibition of ribonucleotide reductase. Cell **112:**391–401. http://dx.doi.org/10.1016/S0092-8674(03)00075-8.

11. **Kumar D, Abdulovic AL, Viberg J, Nilsson AK, Kunkel TA, Chabes A.** 2011. Mechanisms of mutagenesis in vivo due to imbalanced dNTP pools. Nucleic Acids Res **39:**1360–1371.
12. **Weinberg G, Ullman B, Martin DW, Jr.** 1981. Mutator phenotypes in mammalian cell mutants with distinct biochemical defects and abnormal deoxyribonucleoside triphosphate pools. Proc Natl Acad Sci U S A **78:**2447–2451. http://dx.doi.org/10.1073/pnas.78.4.2447.
13. **Mathews CK.** 2006. DNA precursor metabolism and genomic stability. FASEB J **20:**1300–1314. http://dx.doi.org/10.1096/fj.06-5730rev.
14. **Tanaka H, Arakawa H, Yamaguchi T, Shiraishi K, Fukuda S, Matsui K, Takei Y, Nakamura Y.** 2000. A ribonucleotide reductase gene involved in a p53-dependent cell-cycle checkpoint for DNA damage. Nature **404:**42–49. http://dx.doi.org/10.1038/35003506.
15. **Nakano K, Balint E, Ashcroft M, Vousden KH.** 2000. A ribonucleotide reductase gene is a transcriptional target of p53 and p73. Oncogene **19:**4283–4289. http://dx.doi.org/10.1038/sj.onc.1203774.
16. **Niida H, Katsuno Y, Sengoku M, Shimada M, Yukawa M, Ikura M, Ikura T, Kohno K, Shima H, Suzuki H, Tashiro S, Nakanishi M.** 2010. Essential role of Tip60-dependent recruitment of ribonucleotide reductase at DNA damage sites in DNA repair during G_1 phase. Genes Dev **24:**333–338. http://dx.doi.org/10.1101/gad.1863810.
17. **Chabes A, Domkin V, Thelander L.** 1999. Yeast Sml1, a protein inhibitor of ribonucleotide reductase. J Biol Chem **274:**36679–36683. http://dx.doi.org/10.1074/jbc.274.51.36679.
18. **Zhao X, Chabes A, Domkin V, Thelander L, Rothstein R.** 2001. The ribonucleotide reductase inhibitor Sml1 is a new target of the Mec1/Rad53 kinase cascade during growth and in response to DNA damage. EMBO J **20:**3544–3553. http://dx.doi.org/10.1093/emboj/20.13.3544.
19. **Arnaoutov A, Dasso M.** 2014. Enzyme regulation. IRBIT is a novel regulator of ribonucleotide reductase in higher eukaryotes. Science **345:**1512–1515. http://dx.doi.org/10.1126/science.1251550.
20. **Andreson BL, Gupta A, Georgieva BP, Rothstein R.** 2010. The ribonucleotide reductase inhibitor, Sml1, is sequentially phosphorylated, ubiquitylated and degraded in response to DNA damage. Nucleic Acids Res **38:**6490–6501. http://dx.doi.org/10.1093/nar/gkq552.
21. **Lecona E, Barrasa JI, Olmo N, Llorente B, Turnay J, Lizarbe MA.** 2008. Upregulation of annexin A1 expression by butyrate in human colon adenocarcinoma cells: role of p53, NF-Y, and p38 mitogen-activated protein kinase. Mol Cell Biol **28:**4665–4674. http://dx.doi.org/10.1128/MCB.00650-07.
22. **Rodriguez CI, Buchholz F, Galloway J, Sequerra R, Kasper J, Ayala R, Stewart AF, Dymecki SM.** 2000. High-efficiency deleter mice show that FLPe is an alternative to Cre-loxP. Nat Genet **25:**139–140. http://dx.doi.org/10.1038/75973.
23. **Murga M, Bunting S, Montana MF, Soria R, Mulero F, Canamero M, Lee Y, McKinnon PJ, Nussenzweig A, Fernandez-Capetillo O.** 2009. A mouse model of ATR-Seckel shows embryonic replicative stress and accelerated aging. Nat Genet **41:**891–898. http://dx.doi.org/10.1038/ng.420.
24. **Austin WR, Armijo AL, Campbell DO, Singh AS, Hsieh T, Nathanson D, Herschman HR, Phelps ME, Witte ON, Czernin J, Radu CG.** 2012. Nucleoside salvage pathway kinases regulate hematopoiesis by linking nucleotide metabolism with replication stress. J Exp Med **209:**2215–2228. http://dx.doi.org/10.1084/jem.20121061.
25. **Flach J, Bakker ST, Mohrin M, Conroy PC, Pietras EM, Reynaud D, Alvarez S, Diolaiti ME, Ugarte F, Forsberg EC, Le Beau MM, Stohr BA, Mendez J, Morrison CG, Passegue E.** 2014. Replication stress is a potent driver of functional decline in ageing haematopoietic stem cells. Nature **512:**198–202. http://dx.doi.org/10.1038/nature13619.
26. **Taricani L, Shanahan F, Malinao MC, Beaumont M, Parry DA.** 2014. functional approach reveals a genetic and physical interaction between ribonucleotide reductase and CHK1 in mammalian cells. PLoS One **9:**e111714. http://dx.doi.org/10.1371/journal.pone.0111714.
27. **Besse B, Olaussen KA, Soria JC.** 2013. ERCC1 and RRM1: ready for prime time? J Clin Oncol **31:**1050–1060. http://dx.doi.org/10.1200/JCO.2012.43.0900.